Supporting Information

Gautham Nair, Jing Zhao, and Moungi G. Bawendi

January 18, 2011

1 Relationship between n and $g_0^{(2)}$

In this section we derive a relationship between measured correlation histograms and the underlying statistics of photon emission. Without loss of generality, we can begin the calculation at the first pulse *after* the correlator card has finished a single recording. This source will emit a random number n of photons, with a probability distribution $p(n)$. There are a number of possibilities:

1. Start and stop occur during this n-photon emission pulse. Stop can actually occur slightly before start because an electronic cable delay was set up to allow recording of negative start-stop times.

2. Start occurs during this pulse. Stop does not occur in this pulse.

3. Stop occurs during this pulse but start does not.

Option 1 leads to a count at the center peak. If option 2 occurs *and* a stop pulse is detected at the next pulse, there will be a count at the $+t_{rep}$ side peak. Option 3 can only lead to counts at negative-time. We focus on the center peak and the $+t_{rep}$ peak.

The probability of start and stop occuring during the same n-photon pulse is the probability that at least one photon is detected at the start APD and at least one photon is detected at the stop APD. Let N_α and N_β be random variables representing the number of photons detected at the start and the

stop.

$$\begin{aligned} P_n(center) &= P(N_\alpha \geq 1 \,\&\, N_\beta \geq 1) \\ &= 1 - P(N_\alpha = 0 \,\text{or}\, N_\beta = 0) \\ &= 1 - P(N_\alpha = 0) - P(N_\beta = 0) + P(N_\alpha = 0 \,\&\, N_\beta = 0) \\ &= 1 - (1-\alpha)^n - (1-\beta)^n + (1-\alpha-\beta)^n \end{aligned}$$

where α and β are the detection probabilities of an emitted photon at the start and stop channels. These probabilities include all losses from the point of NC emission to the detectors. Importantly, they include the beamsplitter in the detection arm, so that $\alpha + \beta$ can never be > 1. To compute the size of the side peak we note that the probability of start occuring at the n-photon pulse and the stop occuring at the next is the probability that at least one photon is detected at the start APD and *no* photon is detected at the stop multiplied by the probability that at least one photon is detected at the stop APD *at the next pulse*. Let P_β equal this last probability. Then:

$$\begin{aligned} P_n(side) &= P(N_\alpha \geq 1 \,\&\, N_\beta = 0) P_\beta \\ &= \left[P(N_\beta = 0) - P(N_\alpha = 0 \,\&\, N_\beta = 0)\right] P_\beta \\ &= \left[(1-\beta)^n - (1-\alpha-\beta)^n\right] P_\beta \end{aligned}$$

where

$$P_\beta = \sum_{m=0}^{\infty} p(m) P(N_\beta \geq 1) = \sum_{m=0}^{\infty} p(m) \left[1 - (1-\beta)^m\right]$$

By adding the contributions from all possible values of n weighted by their probabilities, we get the total intensities at the center and the side peak:

$$\begin{aligned} center &= \sum p(n) P_n(center) \\ &= \sum p(n) \left[1 - (1-\alpha)^n - (1-\beta)^n + (1-\alpha-\beta)^n\right] \\ side &= \sum p(n) P_n(side) \\ &= \sum p(n) \left[(1-\beta)^n - (1-\alpha-\beta)^n\right] P_\beta \end{aligned}$$

1.1 Low detection efficiency limit

The expressions are simplified in the limit where α and β are $\ll 1$, typical of most experiments.

$$\begin{aligned} 1-(1-\alpha)^n-(1-\beta)^n+(1-\alpha-\beta)^n &\approx n(n-1)\alpha\beta \\ (1-\beta)^n-(1-\alpha-\beta)^n &\approx n\alpha \\ 1-(1-\beta)^m &\approx m\beta \end{aligned} \tag{1}$$

The center and side peak intensities become:

$$center = \alpha\beta\sum_n n(n-1)p(n) \qquad side = \alpha\beta\sum_n np(n)\sum_m mp(m)$$

And the ratio is therefore:

$$\begin{aligned} g_0^{(2)} \equiv \frac{center}{side} &= \left(\sum_{n=2}^{\infty} n(n-1)p(n)\right) / \left(\sum_{n=1}^{\infty} np(n)\right)^2 = \frac{\langle n(n-1)\rangle}{\langle n\rangle^2} \\ &= \frac{2p(2)+6p(3)+\ldots}{(p(1)+2p(2)+3p(3)+\ldots)^2} \end{aligned}$$

If the probability distribution of n changes over time, as in the case of nanocrystal blinking, the histogrammed counts at the center and side peaks are still accumulated separately, so that:

$$center = \alpha\beta\left\langle\sum_n n(n-1)p(n,t)\right\rangle_t \qquad side = \alpha\beta\left\langle\left(\sum_n np(n,t)\right)^2\right\rangle_t$$

Therefore,

$$g_0^{(2)} = \frac{\langle\langle n(n-1)\rangle\rangle_t}{\langle\langle n\rangle^2\rangle_t} \tag{2}$$

where $\langle\cdot\rangle_t$ denote time averages.

2 Nanocrystal emission

A colloidal NC can absorb a random number N of photons from the excitation pulse. Each step in the resulting N-length recombination cascade can occur radiatively or nonradiatively. ξ_m is a random variable that takes the value 1 if the decay of the m-th multiexcitonic state to the $m-1$ multiexcitonic state is radiative, 0 otherwise. Then, the emitted photon number from an NC is given by:

$$n_{\mathrm{dot}} = \sum_m \xi_m I_{N \geq m}$$

Where $I_{N \geq m}$ is an indicator variable equal to 1 if $N \geq m$. We compute the random variable in the numerator of $g_0^{(2)}$:

$$n_{\mathrm{dot}}(n_{\mathrm{dot}} - 1) = 2 \sum_m I_{N \geq m} \sum_{m' < m} \xi_m \xi_{m'}$$

Where we have made use of the fact that $I_{N \geq m} I_{N \geq m'} = I_{N \geq m}$ when $m \geq m'$ and that $\xi_m^2 = \xi_m$. Taking expectation values:

$$g_0^{(2)} = \frac{\langle n_{\mathrm{dot}}(n_{\mathrm{dot}} - 1) \rangle}{\langle n_{\mathrm{dot}} \rangle^2} = \frac{2 \sum_m P_{N \geq m} \sum_{m' < m} \langle \xi_m \xi_{m'} \rangle}{\left(\sum_m P_{N \geq m} \langle \xi_m \rangle \right)^2}$$

Here $P_{N \geq m}$ is the probability that at least m photons are absorbed by the NC. In our experiments the excitation wavelength is well above the exciton energy so the absorption process can be treated as Poissonian, with $P_{N=m} = \frac{\langle N \rangle^m}{m!} \exp(-\langle N \rangle)$. In the limit of low power,

$$\lim_{\langle N \rangle \to 0} g_0^{(2)} = \lim_{\langle N \rangle \to 0} \frac{2 P_{N \geq 2} \langle \xi_2 \xi_1 \rangle}{P_{N \geq 1}^2 \langle \xi_1 \rangle^2} = \frac{\langle \xi_2 \xi_1 \rangle}{\langle \xi_1 \rangle^2}$$

Which is the key result used in the paper. If the NC blinks, we apply Eqn. 2, to obtain:

$$\lim_{\langle N \rangle \to 0} g_0^{(2)} = \frac{\langle \langle \xi_2 \xi_1 \rangle \rangle_t}{\langle \langle \xi_1 \rangle^2 \rangle_t} = \frac{\langle \eta_x(t) \eta_{bx}(t) \rangle_t}{\langle \eta_x(t)^2 \rangle_t}$$

Where $\eta_x(t)$ and $\eta_{bx}(t)$ are the time-varying X and BX quantum yields.

2.1 Approximation of X-BX independence

In the main manuscript, the following approximation is made:

$$\frac{\langle \xi_1 \xi_2 \rangle}{\langle \xi_1 \rangle^2} \approx \frac{\langle \xi_2 \rangle}{\langle \xi_1 \rangle} = \frac{\eta_{bx}}{\eta_x} \tag{3}$$

We justify the approximation $\langle \xi_1 \xi_2 \rangle \approx \langle \xi_1 \rangle \langle \xi_2 \rangle$ as follows. Because ξ are either 0 or 1, we can write $\langle \xi_1 \xi_2 \rangle = \langle \xi_2 \rangle \cdot \langle \xi_1 \rangle|_{\xi_2=1}$. Both possible sources of X-BX quantum yield correlation are not expected to play a big role. If the BX emits there is no local energy release to modify the subsequent X emission $\langle \xi_1 \rangle|_{\xi_2=1} \approx \langle \xi_1 \rangle$. If a hidden stochastic variable like surface quality controls ξ_1 and ξ_2 we expect them to be positively correlated so $\langle \xi_1 \rangle|_{\xi_2=1} \geq \langle \xi_1 \rangle$. However, for our experiments the relevant $\langle \xi_1 \rangle$ is already ≈ 1. Therefore, during bright periods, which contribute almost the entirety of the intensity in the measured $g^{(2)}(\tau)$ histogram, $\langle \xi_1 \xi_2 \rangle \approx \langle \xi_1 \rangle \langle \xi_2 \rangle$.

3 Background effects

The results calculated in 1 can be extended to the case where there are two types of photons. $n = n_{\mathrm{dot}}$ is the photon number from the source of interest and n' is a background source, which has detection probabilities α' and β' at the start and stop detectors. Then,

$$\begin{aligned} \mathit{center} &= \sum p_{nn'} \left[n(n-1)\alpha\beta + n'(n'-1)\alpha'\beta' + nn'(\alpha\beta' + \alpha'\beta) \right] \\ \mathit{side} &= \sum p_{nn'}(n\alpha + n'\alpha') \sum p_{nn'}(n\beta + n'\beta') \end{aligned}$$

and

$$g_0^{(2)} = \frac{\alpha\beta\langle n(n-1)\rangle + \alpha'\beta'\langle n'(n'-1)\rangle + \langle nn'\rangle(\alpha\beta' + \alpha'\beta)}{(\langle n\rangle\alpha + \langle n'\rangle\alpha')(\langle n\rangle\beta + \langle n'\rangle\beta')}$$

We use the facts that $\langle n(n-1)\rangle = g^{(2)}_{0\ \mathrm{dot}}\langle n\rangle^2$ and $\langle n'(n'-1)\rangle = g^{(2)}_{0\ \mathrm{backg}}\langle n\rangle^2$ and assume that n and n' are independant. The fraction of the signal from the extra source in channel 1 is given by $y_1 = \frac{\alpha'\langle n'\rangle}{\alpha\langle n\rangle + \alpha'\langle n'\rangle}$ and similarly $y_2 = \frac{\beta'\langle n'\rangle}{\beta\langle n\rangle + \beta'\langle n'\rangle}$. Thus, we find:

$$g_0^{(2)} = (1-y_1)(1-y_2)g_{0\,\mathrm{dot}}^{(2)} + y_1 y_2 g_{0\,\mathrm{backg}}^{(2)} + (1-y_1)y_2 + (1-y_2)y_1 \quad (4)$$

For the case where n' is simply a Poissonian background, as would be the case for laser scatter, etc., then $g_{0\,\mathrm{backg}}^{(2)} = 1$ and we obtain:

$$g_0^{(2)} = 1 + (1-\mathfrak{b}_1)(1-\mathfrak{b}_2)\left[g_{0\,\mathrm{dot}}^{(2)} - 1\right] \quad (5)$$

Where $\mathfrak{b}_{(1,2)} = y_{1,2}$ are the background to total signal ratios. If instead n' is due to another NC, which we assume for simplicity has an identical $g_{0\,\mathrm{backg}}^{(2)} = g_{0\,\mathrm{dot}}^{(2)}$, then we obtain:

$$g_0^{(2)} = g_{0\,\mathrm{dot}}^{(2)} + (x_1 y_2 + x_2 y_1)\left[1 - g_{0\,\mathrm{dot}}^{(2)}\right] \quad (6)$$

where $x_{1,2} = 1 - y_{1,2}$ and $y_{1,2}$ are the signal fractions of the dot of interest and the additional NC in each channel. The results in Eqns. 5 and 6 can be combined, and if the signal fractions from background or other NCs is small one obtains:

$$g_0^{(2)} \approx g_{0\,\mathrm{dot}}^{(2)} + \mathfrak{b}_1 + y_1 + \mathfrak{b}_2 + y_2 \quad (7)$$

By examining intensity time traces of each channel we could estimate an upper bound on the total signal fraction from extraneous sources in the start and stop channels, $Y_1 = \mathfrak{b}_1 + y_1$ and $Y_2 = \mathfrak{b}_2 + y_2$. We found that $Y_1 + Y_2 < 0.015$, significantly lower than most of the $g_0^{(2)}$ values we measured.

4 Calculation of Radiative and Auger rates

In the main text we computed the evolution of $g_0^{(2)}$ for an NC using a simple model to estimate the multiexciton quantum efficiencies $\eta_m = \langle \xi_m \rangle$. We note that $\eta_m = k_m^{rad}\tau_m$. We assume that the multiexciton lifetimes are dominated by the Auger mechanism. By counting the number of possible trion recombination pathways and assuming every trion's recombination occurs with the same rate, one finds that the Auger rate for multiexcitons scales as $k_m \propto m^2(m-1)$ ("Statistical" case in Ref. [1]).

To estimate the radiative rates we ignore fine structure effects and use the simplest model of the band edge electronic structure in CdSe-like NCs. The conduction band states are spatially the same but have the minimum

$S = \frac{1}{2}$ spin degeneracy. The four valence states have mixed spin and orbital angular momentum $F = L_h + J = \frac{3}{2}$ [2]. The spontaneous recombination rate of an electron and hole is proportional to the square of the transition dipole $|\langle\psi_h|\vec{\mu}|\psi_e\rangle|^2$ which can be computed by straightforward application of the Wigner-Eckart theorem. The nonzero matrix elements for recombination with a $m_e = 1/2$ electron are:

$$\begin{aligned}
\left|\left\langle 3/2, 3/2 \left| \mu_1^{(1)} \right| 1/2, 1/2 \right\rangle\right|^2 &= k^{rad} \\
\left|\left\langle 3/2, 1/2 \left| \mu_0^{(1)} \right| 1/2, 1/2 \right\rangle\right|^2 &= \frac{2}{3}k^{rad} \\
\left|\left\langle 3/2, -1/2 \left| \mu_{-1}^{(1)} \right| 1/2, 1/2 \right\rangle\right|^2 &= \frac{1}{3}k^{rad}
\end{aligned}$$

Where k^{rad} is some constant. An average over all four hole states therefore gives $k_X^{rad} = k^{rad}/2$. To compute the BX rate we add up all possible e-h recombination pathways and find that all configurations have $k_{BX}^{rad} = 2k^{rad}$. For $m > 2$ states like the TX, we note that in our experiment we observe chiefly the band-edge fluorescence, so the radiative rates that apply are the rates of $1S_e1S_{3/2}$ emission only. Assuming Aufbau configurations at the band edge of 2e-3h and 2e-4h for $m = 3$ and $m \geq 4$, we compute $k_{TX}^{rad} = 3k^{rad}$ and $k_{\geq 4X}^{rad} = 4k^{rad}$. Combining this with the Auger rate scaling, we can estimate the band-edge emission quantum yields of all higher multiexcitons from the biexciton QY:

$$\eta_m \approx \frac{2\min(m,4)}{m^2(m-1)}\eta_{bx} \tag{8}$$

We show in addition that the BX radiative rate is unaffected by fine structure effects. The results above were obtained using $|\psi_j^{bx}\rangle$ and $|\psi_i^x\rangle$ in the occupation number basis derived from the $S = \frac{1}{2}$ electron and $F = \frac{3}{2}$ hole single particle states. When fine structure effects like e-h coulomb exchange are included, the true eigenstates $|\psi_\alpha^{bx}\rangle$ and $|\psi_\beta^x\rangle$ are a superposition of the occupation-number states. The radiative rate of any of the BX states is proportional to:

$$k_{BX,\alpha}^{rad} = \sum_\beta \sum_{m=-1,0,1} |\langle\psi_\beta^x|\mu_m^{(1)}|\psi_\alpha^{bx}\rangle|^2 = \sum_{m=-1,0,1} \langle\psi_\alpha^{bx}|\mu_m^{(1)} P_x \mu_m^{(1)}|\psi_\alpha^{bx}\rangle$$

Where P_x is the projection operator onto the X subspace. If we choose the occupation number basis to represent $\mu_m^{(1)}$ we note that each of the three matrices $\mu_m^{(1)} P_x \mu_m^{(1)}$ are diagonal because any of the $\mu_m^{(1)}$ connect any of the $|\psi_i^x\rangle$ to at most one $|\psi_j^{bx}\rangle$. Therefore, the matrix $\mu^2 \equiv \sum_m \mu_m^{(1)} P_x \mu_m^{(1)}$ is also diagonal in the $\{|\psi_j^{bx}\rangle\}$ basis, with all the diagonal elements $= 2k^{rad}$, as discussed previously. Writing $|\psi_\alpha^{bx}\rangle = \sum c_j |\psi_j^{bx}\rangle$,

$$k_{BX,\alpha}^{rad} = \sum_{j,j\prime} c_{j\prime}^* c_j \langle \psi_{j\prime}^{bx} | \mu^2 | \psi_j^{bx} \rangle = 2k^{rad} \sum_j |c_j|^2 = 2k^{rad}$$

This proves that fine structure effects play little role in BX radiation at any temperature. The result holds as long as the Wigner-Eckart theorem holds (i.e. there is not too much anisotropy) and as long as it is fair to assume that no other higher conduction or valence band states are involved.

5 Disaggregated $g_0^{(2)}$ data on individual NCs

We show in the Fig. 1 the average $g_0^{(2)}$ for all NCs we measured. The only data point we have excluded from our report was a single measurement on a dot from sample (e) which showed an extremely short X lifetime of ≈ 6 ns, poor, multi-state blinking, and low emission intensity.

6 CW Antibunching on NCs

Consider the three level system formed by ground, exciton and biexciton states. The photon absorption rate is γ and the decay rates of X and BX are k_1 and k_2 respectively. Then:

$$\frac{\mathrm{d}}{\mathrm{d}t} \begin{bmatrix} \sigma_2 \\ \sigma_1 \\ \sigma_0 \end{bmatrix} = \begin{bmatrix} -k_2 & \gamma & 0 \\ k_2 & -\gamma - k_1 & \gamma \\ 0 & k_1 & -\gamma \end{bmatrix} \begin{bmatrix} \sigma_2 \\ \sigma_1 \\ \sigma_0 \end{bmatrix}$$

The system has three eigenvectors, the first of which corresponds to equilibrium:

$$\lambda_0 = 0 \quad \boldsymbol{\sigma}_{eq} = \frac{1}{k_1 + \gamma + \gamma^2/k_2} \begin{bmatrix} \gamma^2/k_2 \\ \gamma \\ k_1 \end{bmatrix}$$

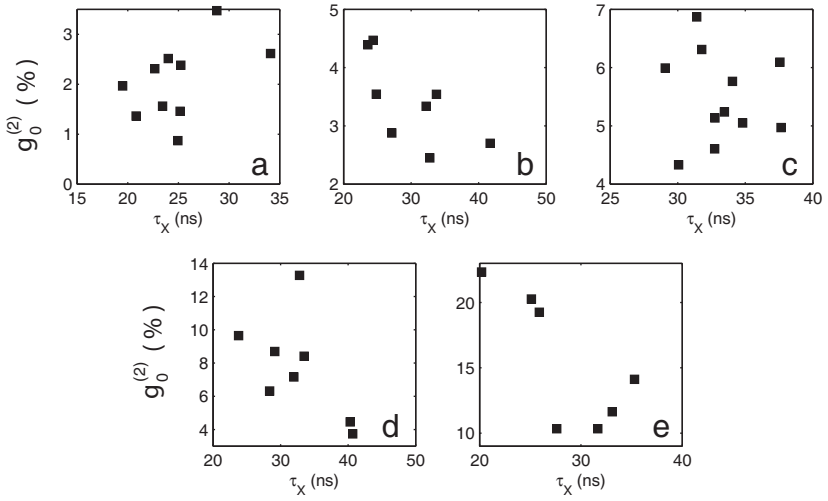

Figure 1: Plot of measured $g_0^{(2)}$ against the X lifetime τ_x obtained from fitting the shape of the peaks in $g^{(2)}(\tau)$ for the individual dots we measured in each sample. The ensemble BX lifetime of samples (a) through (e) are 60, 130, 330, 420, and 920 ps. We observe that, in general, τ_X does not account for the variation in $g_0^{(2)}$ within any of the samples

The measured photon cross-correlation $g^{(2)}(t)$ is proportional to the probability density of detecting a photon at time t given that a photon has been detected at time 0. If photons can be attributed to either X or BX emission, $g^{(2)}(t)$ can be decomposed as follows:

$$\begin{aligned} g^{(2)}(t) &\propto P(\text{detect } h\nu \text{ at } t|\text{detect } h\nu \text{ at } 0) \\ &= P(h\nu \text{ at } t|\text{X } h\nu \text{ at } 0) \times \frac{I_X}{I_{total}} \\ &\quad + P(h\nu \text{ at } t|\text{BX } h\nu \text{ at } 0) \times \frac{I_{BX}}{I_{total}} \end{aligned}$$

Each one of the possible t=0 events prepares the system in a particular state. If an X photon is detected, the system is in the ground state, while if BX photon is detected, the system is in the X state. The light intensity is described by:

$$I(t) = \left[\begin{array}{ccc} \eta_{bx}k_2 & \eta_x k_1 & 0 \end{array} \right] \cdot \boldsymbol{\sigma}(t)$$

At steady state $\boldsymbol{\sigma}(t) = \boldsymbol{\sigma}_{eq}$:

$$I_{total} = \underbrace{\frac{\eta_{bx}\gamma^2}{k_1 + \gamma + \gamma^2/k_2}}_{I_{BX}} + \underbrace{\frac{\eta_x k_1 \gamma}{k_1 + \gamma + \gamma^2/k_2}}_{I_X}$$

Then,

$$g^{(2)}(0) \propto I_{BX} \left[\begin{array}{ccc} \eta_{bx}k_2 & \eta_x k_1 & 0 \end{array} \right] \cdot \left[\begin{array}{c} 0 \\ 1 \\ 0 \end{array} \right] + I_X \left[\begin{array}{ccc} \eta_{bx}k_2 & \eta_x k_1 & 0 \end{array} \right] \cdot \left[\begin{array}{c} 0 \\ 0 \\ 1 \end{array} \right]$$

Dividing by $g^{(2)}(\infty) \propto (I_{BX} + I_X)^2$ for proper normalization, we find:

$$\frac{g^{(2)}(0)}{g^{(2)}(\infty)} = \frac{I_{BX}\eta_x k_1}{(I_X + I_{BX})^2} = \frac{\eta_{bx}}{\eta_x} \times \frac{1 + \frac{\gamma}{k_1} + \frac{\gamma^2}{k_2 k_1}}{\left(1 + \frac{\gamma}{k_1}\frac{\eta_{bx}}{\eta_x}\right)^2} \approx \frac{\eta_{bx}}{\eta_x} \text{ for } \gamma \ll k_1$$

The condition $\gamma \ll k_1$ is readily satisfied in most experiments. The result that $g^{(2)}(0)/g^{(2)}(\infty) = \eta_{bx}/\eta_x$ under weak CW excitation is analogous to our earlier result that $g_0^{(2)} = \eta_{bx}/\eta_x$ under weak pulsed excitation. In either scenario, biexciton luminescence limits the depth of antibunching.

7 BX lifetimes and QY from ensemble tPL

We determined the characteristic BX lifetime of each sample by transient photoluminescence spectroscopy of ensembles of NCs. Hexane dispersions of nanocrystals were excited with 400nm pulses derived from a 1kHz amplified Ti:sapphire laser. The photoluminescence was collected, directed to a monochromator, and dispersed onto a Hamamatsu C5680 streak camera. Samples were stirred and kept at room temperature in air.

Figure 2 shows representative PL decays under high excitation fluence for each of the five samples studied. The fitting method follows that described in our previous work [3]. Decays at high power are fit to a functional form $a_{BX}e^{-k_{BX}t} + a_X f(t)$, where the X dynamics, $f(t)$, is an exponential or biexponential fitted to PL decays obtained under weak excitation. As in our previous work, to reduce the influence of faster decay components from higher multiexcitons on our estimated τ_{BX}, we fit only times $t > \approx \tau_{BX}/2$. We have shown that this procedure results in values of τ_{BX} that are consistent across an excitation power series [3]. The BX lifetimes averaged over several measurements for samples (a)-(e) are 60, 130, 330, 420, and 920 ps respectively.

The ensemble BX QY of the QDOT655 sample that was later used in this work was found to be $\eta_{bx} \approx 0.11$ by Fisher et al.[4] We also obtain $\eta_{bx} \approx 0.12$ for this sample using our ensemble value of $\tau_{BX} \approx 920$ ps, the average single NC $\tau_X \approx 30$ ns which is $\approx \tau_X^{rad}$ since $\eta_x^{on} \approx 1$ and the relationship $k_{BX}^{rad} \approx 4k_X^{rad}$. [3]

8 Effect of Auger lifetime inhomogeneity on ensemble BX decays

Our experiments show that individual nanocrystals from an ensemble exhibit slightly different biexciton quantum yields. We attribute this to dot-to-dot inhomogeneity of the BX lifetimes. However, ensemble BX decays are apparently well fit by single exponential decays. We discuss here that this is related to the type and extent of the inhomogeneity.

The BX QYs measured for single NCs were always within a factor of two or less of the average BX QY for the ensemble. Then, the distribution of the BX decay rates (we use rates instead of lifetimes for computational

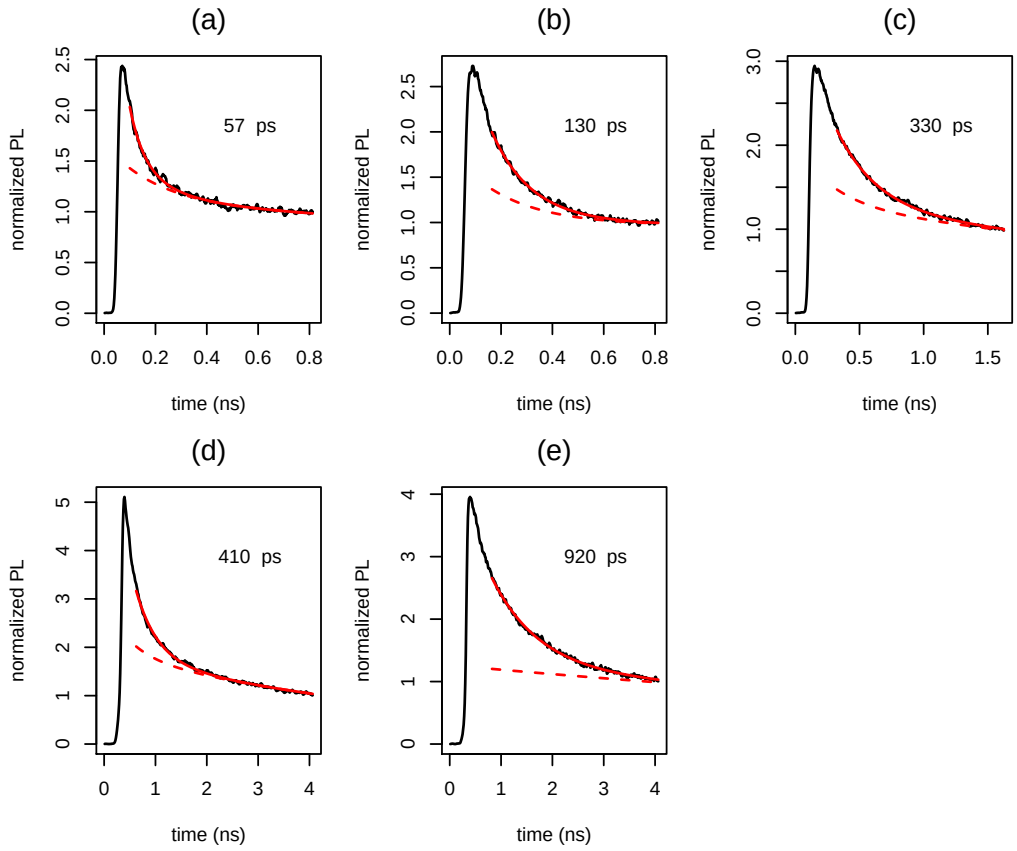

Figure 2: (a)-(e) Fits of representative ensemble transient PL data collected for each of the five samples studied in this work under strong 400nm pulsed excitation. Black lines are experimental decays, normalized at long times. Red solid lines are fits to the form $a_{BX}e^{-k_{BX}t} + a_X f(t)$, where $f(t)$ represents the X dynamics as described in the text. The dashed red lines are the $a_X f(t)$ component of the fit. The BX lifetime estimated, $\tau_{BX} = k_{BX}^{-1}$, is shown in each plot. Fits begin at $t \approx \tau_{BX}/2$ to avoid artifacts from higher multiexcitons.

convenience) in the sample can be modeled as a uniform distribution: [1]

$$\rho_{bx}(k) = \begin{cases} 0 & \text{if } k < k_0 - \Delta k \\ \frac{1}{2\Delta k} & \text{if } |k - k_0| \leq \Delta k \\ 0 & \text{if } k > k_0 + \Delta k \end{cases} \tag{9}$$

The corresponding ensemble photoluminescence decay $s(t)$ is given by:

$$s(t) = \int e^{-kt} \rho_{bx}(k) = e^{-k_0 t} \frac{\sinh(\Delta k t)}{\Delta k t} \tag{10}$$

The decay differs from a single exponential by a multiplicative factor $f(\Delta k t) = \frac{\sinh(\Delta k t}{\Delta k t}$. This is nearly $= 1$ for $t \ll (\Delta k)^{-1}$ and only increases by 20% for $t \approx (\Delta k)^{-1}$ (Fig. 3(a)). The inhomogeneity in decay rates only affects the long tail of the measured decay. Figures 3(b-c) illustrate this for a population in which the full spread $2\Delta k$ of decay rates is of the same size as the average decay rate itself, k_0. This inhomogeneity is more severe than that found from our single dot BX QY data. It is seen that the deviation from single exponential dynamics only affects the long tail of the ensemble BX decay. The effect is difficult to observe in tPL because of limited signal to noise and overlap with the X decay.

References

[1] V. I. Klimov, J. A. McGuire, R. D. Schaller, and V. I. Rupasov, *Phys. Rev. B* **77**, 195324 (2008).

[2] D. J. Norris and M. G. Bawendi, *Phys. Rev. B* **53**, 16338 (1996).

[3] G. Nair and M. G. Bawendi, *Phys. Rev. B* **76**, 081304(R) (2007).

[4] B. R. Fisher, J.-M. Caruge, D. Zehnder, and M. G. Bawendi, *Phys. Rev. Lett.* **94**, 087403 (2005).

[1] This contrasts with the X lifetimes of some NC samples in which subpopulations can have lifetimes of less than 100 ps while the average is on the order of 10 ns.

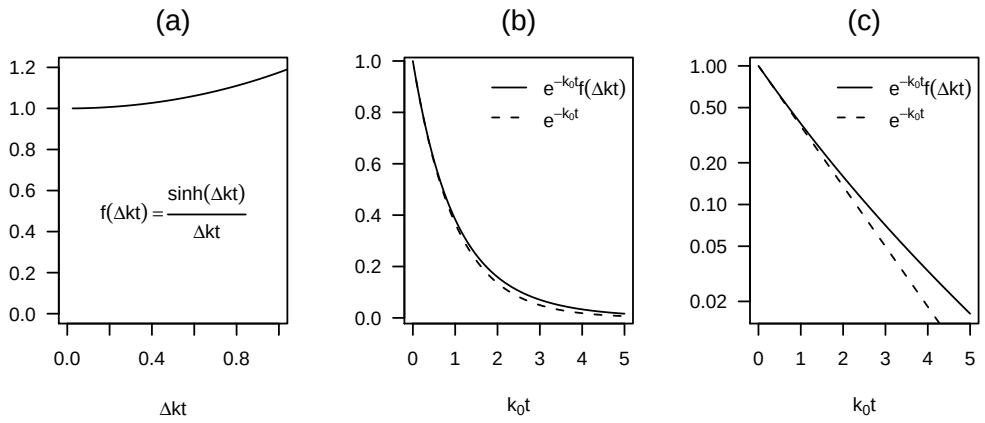

Figure 3: (a) Plot of the multiplicative factor that causes $s(t)$ to deviate from a single exponential if the distribution of decay rates is uniform with full width $2\Delta k$. The deviation is small as long as Δkt is comparable or smaller than 1. (b) Plot of a model decay for the case $2\Delta k = k_0$. Dashed line is a single exponential decay without the inhomogeneity. (c) Same as (b) but on log scale